

# Advanced CLARITY for rapid and high-resolution imaging of intact tissues

Raju Tomer<sup>1–3</sup>, Li Ye<sup>1–3</sup>, Brian Hsueh<sup>1,3</sup> & Karl Deisseroth<sup>1–4</sup>

<sup>1</sup>Department of Bioengineering, Stanford University, Stanford, California, USA. <sup>2</sup>Howard Hughes Medical Institute, Stanford University, Stanford, California, USA.

<sup>3</sup>CNC Program, Stanford University, Stanford, California, USA. <sup>4</sup>Department of Psychiatry and Behavioral Sciences, Stanford University, Stanford, California, USA.

Correspondence should be addressed to K.D. ([deissero@stanford.edu](mailto:deissero@stanford.edu)).

Published online 19 June 2014; doi:10.1038/nprot.2014.123

**CLARITY is a method for chemical transformation of intact biological tissues into a hydrogel-tissue hybrid, which becomes amenable to interrogation with light and macromolecular labels while retaining fine structure and native biological molecules. This emerging accessibility of information from large intact samples has created both new opportunities and new challenges. Here we describe protocols spanning multiple dimensions of the CLARITY workflow, ranging from simple, reliable and efficient lipid removal without electrophoretic instrumentation (passive CLARITY) to optimized objectives and integration with light-sheet optics (CLARITY-optimized light-sheet microscopy (COLM)) for accelerating data collection from clarified samples by several orders of magnitude while maintaining or increasing quality and resolution. The entire protocol takes from 7–28 d to complete for an adult mouse brain, including hydrogel embedding, full lipid removal, whole-brain antibody staining (which, if needed, accounts for 7–10 of the days), and whole-brain high-resolution imaging; timing within this window depends on the choice of lipid removal options, on the size of the tissue, and on the number and type of immunostaining rounds performed. This protocol has been successfully applied to the study of adult mouse, adult zebrafish and adult human brains, and it may find many other applications in the structural and molecular analysis of large assembled biological systems.**

## INTRODUCTION

One goal of modern neuroscience is to map the architecture of neural circuits with both high (wiring-level) resolution and broad (brainwide) perspective. This challenge has drawn the attention of generations of scientists, beginning in the nineteenth century with Ramón y Cajal's detailed representations of neurons visualized at high resolution with the Golgi staining technique while still embedded within semi-intact brain tissue. Principles fundamental to the understanding of neural systems can result from such an integrative approach, but although progress has been made, many challenges and opportunities remain.

Over the past few decades, electron microscopy (EM) has emerged as a foundational method for deciphering details of neuronal circuit structure<sup>1,2</sup>. The key advantage of EM in this regard (relative to light microscopy) is the identification of presynaptic active zones containing neurotransmitter vesicles apposed to postsynaptic structures. In addition, EM facilitates visualization of some of the finest branches of axons. However, EM tissue mapping requires relatively slow steps involving ultrathin sectioning and/or ablation, and reconstruction; most importantly, the sample contrast preparation is largely incompatible with rich molecular phenotyping that could provide critical information on cell and synapse type. Ideally, data sets resulting from intact-brain mapping should be linkable to molecular information on the types of cells and synapses that are imaged structurally, and even to dynamic information on natural activity pattern history (in these same circuits) known to be causally relevant to animal behavior. Suitable light-based imaging approaches, combined with specific genetic or histochemical molecular labeling methods, have emerged as important tools for visualizing the structural, molecular and functional architecture of biological tissues, with a particularly vital role in emerging brainwide, high-resolution neuroanatomy.

Confocal methods revolutionized light microscopy by enabling optical sectioning in thick (tens of micrometers) fluorescently

labeled samples, thereby allowing 3D reconstruction without the need for ultrathin physical sectioning<sup>3</sup>. Two-photon microscopy further increased the accessible imaging depth (to hundreds of micrometers) even in living tissue samples<sup>4</sup>, and adaptive-optics approaches have improved imaging depth further<sup>5</sup>. However, light microscopy remains limited for imaging throughout intact vertebrate nervous systems (for example, mouse brains span many millimeters even in the shortest spatial dimension, and they are opaque on this scale chiefly owing to light scattering). A common work-around to this limitation has been to slice brains into thin sections, in a manual or automated fashion, followed by confocal or two-photon imaging<sup>6,7</sup>; however, detailed labeling and reconstruction from thin sections has been (so far) limited to small volumes of tissue. An ideal integrative approach would be to label and image entirely intact vertebrate brains at high resolution.

As a step in this direction, new methods have emerged to increase tissue transparency<sup>8–10</sup> by chemically reducing the scattering of light traveling through the tissue sample. Although intriguing and effective, these approaches are not generally suitable for detailed molecular phenotyping, as most tissues (such as the intact mature brain) remain largely impenetrable to macromolecular antibody or oligonucleotide labels<sup>11</sup>. When pieces of soft tissue such as mammary glands can be stained using hydrophobic clearing solutions that reduce lipid barriers to antibody labeling<sup>12</sup>, fluorophores become highly unstable or quenched in the clearing process (a step that nevertheless must follow the antibody-staining phase, as transparency is otherwise lost<sup>12</sup>). These limitations motivated the recent development of CLARITY<sup>11,13</sup>, which involves the removal of lipids in a stable hydrophilic chemical environment to achieve transparency of intact tissue, preservation of ultrastructure and fluorescence, and accessibility of native biomolecular content to antibody and nucleic acid probes. Subsequent screens for diverse hydrophilic lipid solubilization compounds have been productive and can be integrated with

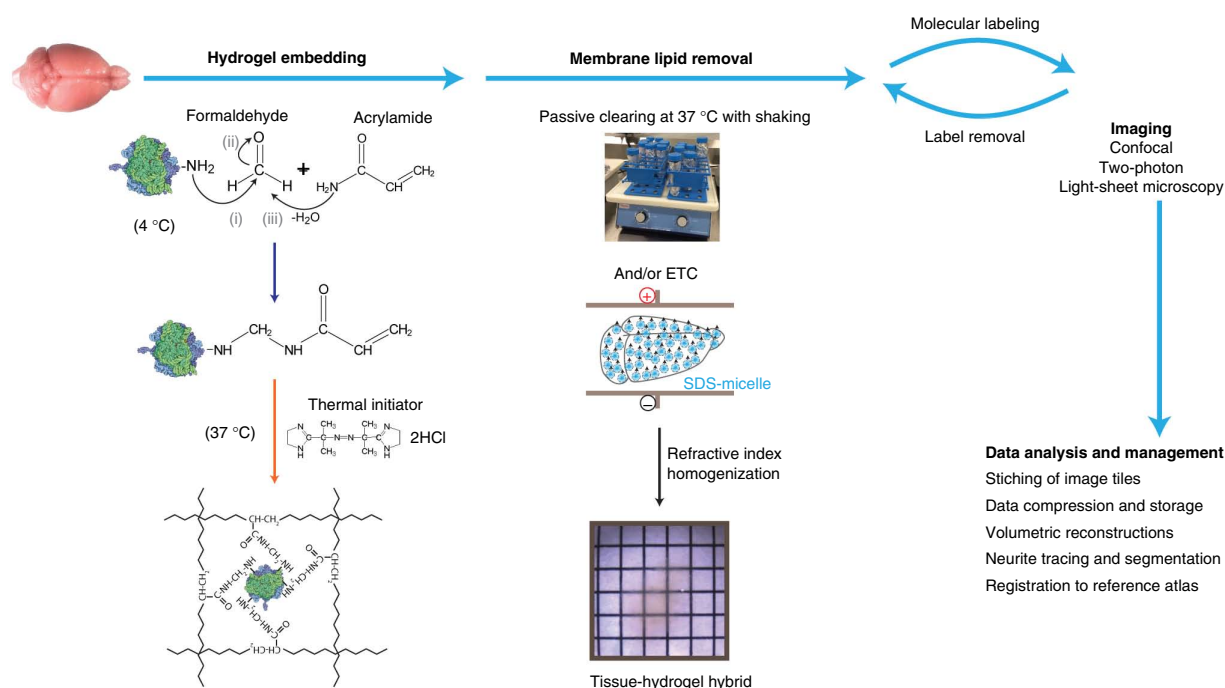


**Figure 1** | CLARITY pipeline overview. The tissue sample, e.g., an intact mouse brain, is perfused with cold HM solution that contains a cocktail of acrylamide, bisacrylamide, formaldehyde and thermal initiator. Formaldehyde mediates cross-linking of biomolecules to acrylamide monomers via amine groups; presumptive chemistry of this process is shown. Hydrogel polymerization is initiated by incubating the perfused tissue at 37 °C, resulting in a meshwork of fibers that preserves biomolecules and structural integrity of the tissue. Lipid membranes are removed by passive thermal clearing in SBC solution at 37 °C or by ETC. The resulting intact tissue-hydrogel hybrid can undergo multiple rounds of molecular and structural interrogation using immunohistochemistry and light microscopy. A dedicated computational infrastructure is needed to analyze and store the data. All animal experiments were carried out with Stanford University Institutional review panel approval.

CLARITY<sup>14</sup>. The CLARITY technical platform enables multiple rounds of molecular, structural and activity-history interrogation throughout intact adult mammalian brains; this is of relevance

not only for neuroscience but also for research into any intact biological system. Thus far, CLARITY has been used to interrogate mouse brains, adult zebrafish and postmortem human

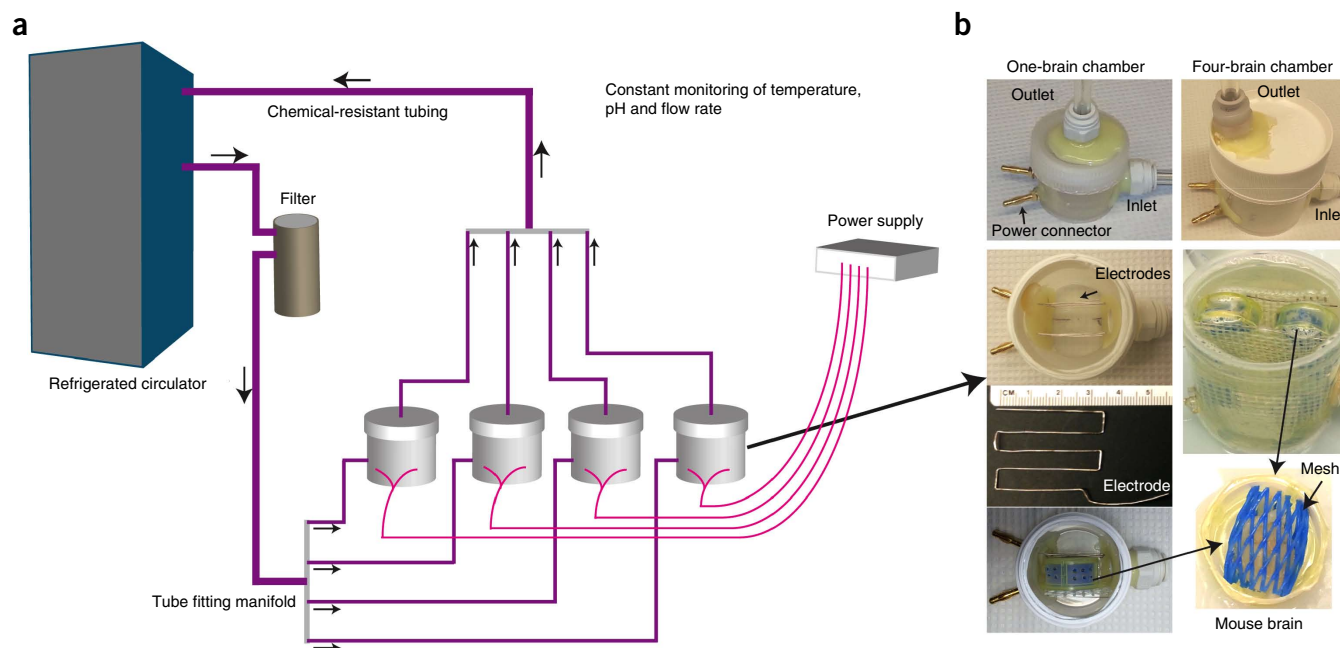
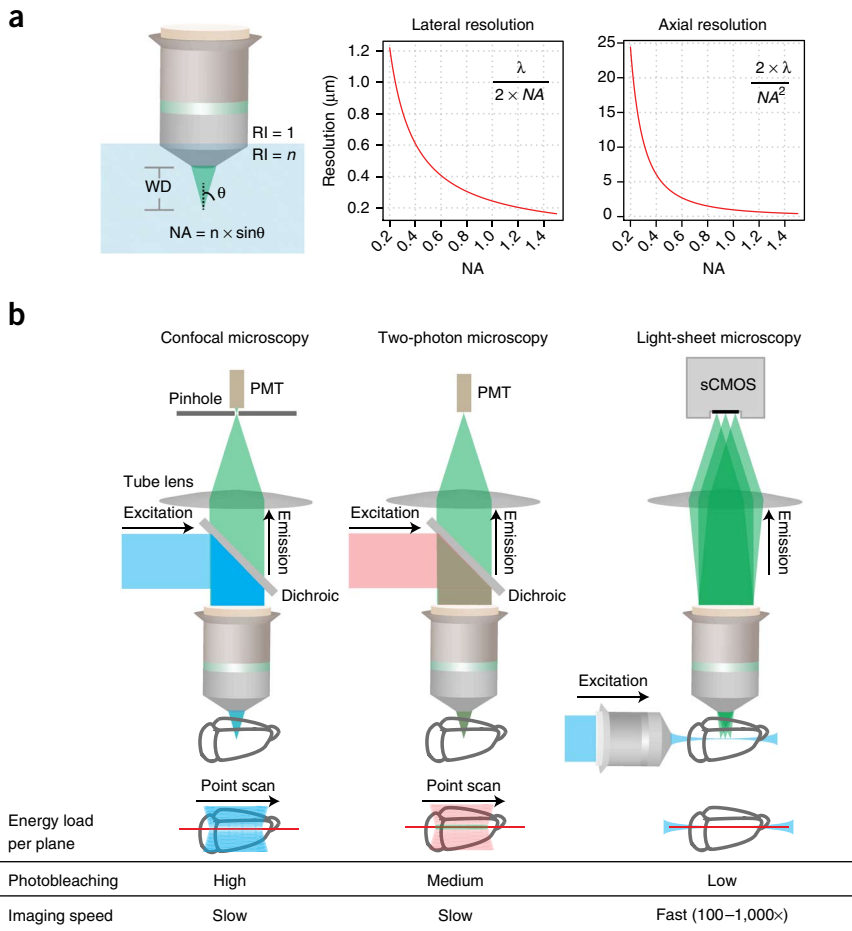


**Figure 2** | ETC. (a) Schematic of a multiplexed ETC setup. (b) Implementation of two differently sized ETC chambers fitting one brain (left) or up to four brains (right). Top pair of images, the two chambers are constructed similarly with regard to power and fluid inlet and outlet. Second image at left, internal arrangement of electrodes. Third image at left, dimension of electrode geometry: note the centimeter ruler for scale. Fourth image at left, positioning of a brain in the single-brain chamber. Second image at right, positioning of four brains in the multi-brain chamber. Third image at right, closeup of nonmetallic mesh for brain positioning: similar composition and positioning for both chambers.

**Figure 3 |** Imaging clarified samples. (a) Key microscope objective parameters relevant to CLARITY are WD, NA, RI ( $n$ ) and multicolor correction. WD is the distance between the objective lens and the focal plane. NA relates to the fraction of total emitted signal collected by an objective, and higher NA enables higher resolution. The graphs plot diffraction-limited lateral and axial resolution parameters as a function of NA, assuming  $\lambda = 500$  nm.

(b) Comparison of confocal, two-photon and light-sheet microscopy. Confocal microscopy achieves optical sectioning by using a pinhole in front of the photomultiplier tubes (PMTs). Two-photon microscopy uses the fact that only simultaneous absorption of two photons (of longer wavelengths) results in fluorescence signal emission, an event that is more likely to occur at the point of highest light intensity in the sample, i.e., the focal plane. Light-sheet fluorescence microscopy achieves optical sectioning by selectively confining the illumination to the plane of interest. Confocal microscopy and two-photon microscopy are point scanning and hence inherently slow, whereas light-sheet microscopy uses fast sCMOS or CCD cameras to image the selectively illuminated focal plane, resulting in minimal photobleaching and imaging speed that is 2–3 orders of magnitude faster than point-scanning methods.



brain tissue<sup>13</sup>, but we anticipate that the protocol can be adapted to other tissues. In anticipation of the wide range of potential applications, we refer readers to the active discussion forum established for further optimization of the technique (<http://forum.claritytechniques.org/>).

### Clarifying large tissue volumes

CLARITY builds on chemical principles to grow hydrogel polymers from inside the tissue in order to provide a support framework for structural and biomolecular content (Fig. 1). This is achieved first by infusing a cold (4 °C) cocktail of hydrogel monomers (HMs; for example, acrylamide with bisacrylamide, but other types of monomers may also be used<sup>11</sup>), formaldehyde and thermally triggered initiators into the tissue, followed by polymerization of the hydrogel at 37 °C. Formaldehyde serves the dual purposes of cross-linking amine-containing tissue components to each other and covalently binding the HMs to these native biomolecules, which include proteins, nucleic acids and other small molecules (Fig. 1), but not the vast majority of cellular membrane phospholipids. After the hydrogel polymerization is triggered, lipids (responsible for preventing access of both photons and molecular labels to deep structures) can then be readily removed without destroying or losing native tissue components using strong ionic detergent-based clearing solution (borate-buffered 4% (wt/vol) SDS) at 37 °C, either passively with gentle recirculation or with active electrophoretic forcing (the latter greatly accelerates but introduces some experimental complexity and risk; Fig. 2). The resulting lipid-extracted and structurally stable tissue-hydrogel hybrid is immersed in a refractive index (RI) homogenization solution (such as 85–87% (vol/vol) glycerol or FocusClear, RI ~1.454 as shown in ref. 13, although best results

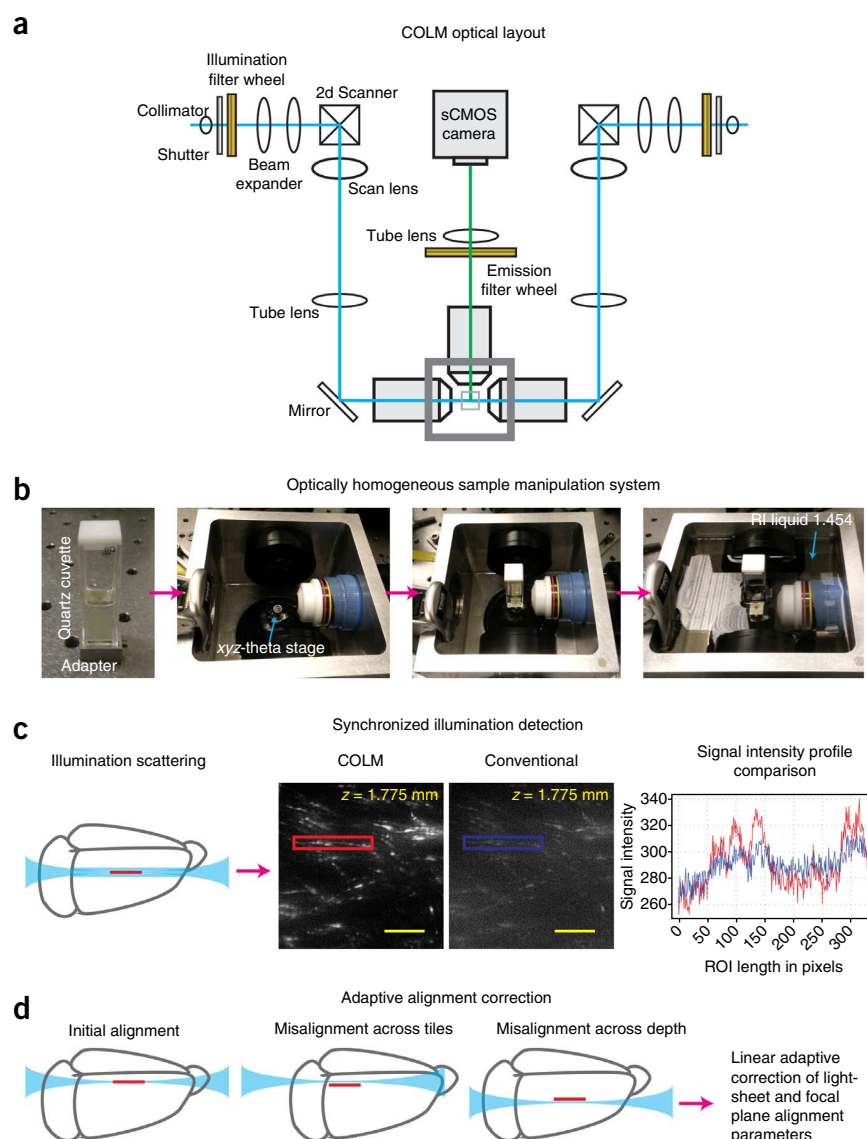
are achieved with FocusClear<sup>13</sup>) to render the intact brain transparent to light (Fig. 1 and Supplementary Fig. 1).

An additional feature of the stable hydrogel-tissue hybrid is that it can be subjected to multiple rounds of molecular interrogation. Typically, immunohistochemistry methods only allow investigation of two or three biomarkers at once in a tissue sample, but more simultaneous labels are required to define cells in terms of precise molecular and genetic identity, wiring and activity history. This limitation is traditionally approached by combining information from multiple samples into a standard reference atlas. However, this strategy fails to fully phenotype individual cells, cannot capture the joint statistics among the different kinds of labels within a single preparation and suffers from 3D alignment artifacts and variability among different individual tissue samples. By allowing multiple rounds of histochemical labeling and elution in the same tissue, CLARITY provides unusually rich access to molecular and structural information.

### Imaging large clarified tissue volumes

The next major challenge after achieving access to clarified large tissues is to develop optimized and high-resolution deep-imaging approaches. One of the most important components of any light microscopy system is the detection objective (Fig. 3a), which sets the resolution that can be achieved and the maximum sample size that can be imaged. In this context, three critical parameters of a detection objective are as follows: (i) working distance (WD), (ii) numerical aperture (NA) and (iii) optical aberration (color) correction, for multiple light wavelengths and immersion-medium

**Figure 4 | COLM for large intact samples.** (a) Optical layout of the CLARITY-optimized light-sheet microscope. Two light sheets are created from opposite sides; shown are galvanometer scanners, scan lens, tube lens and illumination objectives. The emitted fluorescence is imaged with an in-focus detection objective, tube lens and sCMOS camera. Illumination and emission filter wheels (motorized) are used to generate well-defined excitation light and emission signal bands, respectively. The innovations required for COLM are discussed in **b–d**, and a schematic is shown in **Supplementary Figure 2**. (b) Optically homogeneous sample mounting framework for large intact samples. Clarified samples, such as intact adult mouse brain, are mounted in a quartz cuvette filled with RI matching solution such as FocusClear. Note that the RI of quartz glass (~1.458) is nearly identical to that of FocusClear (~1.454). A bottom adapter is used to attach the cuvette to the xyz-theta stage in the sample chamber, which is then filled with a matching RI liquid (~1.454). This results in an optically homogeneous sample manipulation system with minimal RI transition boundaries. (c) Synchronized illumination and detection is achieved by synchronizing the scanning beam with the unidirectional readout of a sCMOS camera chip, resulting in a virtual-slit effect that allows substantially improved imaging quality, as illustrated by the images shown acquired from the same plane with COLM and with conventional light-sheet microscopy. The graph at right compares the signal intensity profile of a field acquired with COLM (red) and conventional light-sheet microscopy (blue). (d) Large clarified samples can have marked RI inhomogeneity, resulting in the need for correction of misalignment of illumination with the focal plane of the detection objective. We achieve this with a linear adaptive calibration procedure before starting the imaging experiment, as described in Step 22B. Scale bars, 100  $\mu\text{m}$ .

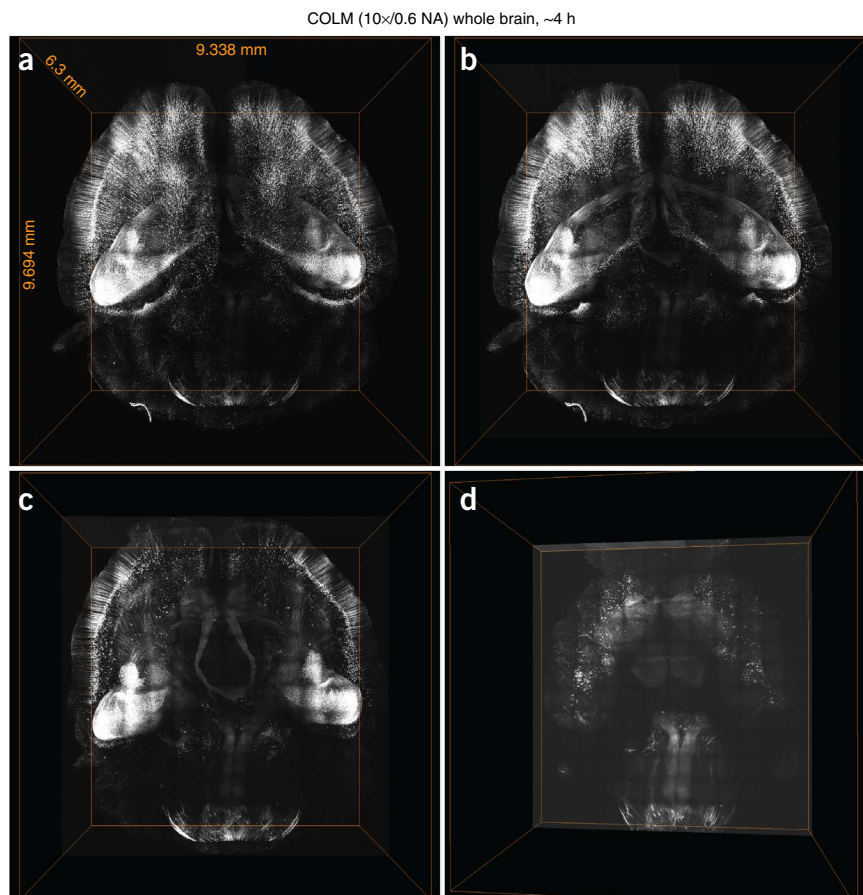


RI (Fig. 3a). WD is the distance between the focal plane (or the imaging plane) and the physical edge of the objective lens, and it therefore determines how deep one can image without physically touching the sample. NA describes how much of the emitted fluorescence signal can be collected by the objective and the diffraction-limited resolution that can be achieved (higher NA translates to improved resolution in a wavelength-dependent manner, according to the relationship defined by the Abbe diffraction limit of  $\lambda/2\text{NA}$ ; Fig. 2a). In addition, the level of aberration correction defines, among other aspects, how well the acquired multicolor images are co-registered. There are trade-offs among these three parameters, and for imaging large clarified samples the investigator must strike a scientific question-guided balance constrained by the nature of the specific experimental system. Finally, the selected properties must be integrated in a microscope objective matched to the RI range of the immersion liquid and the tissue sample, which is a property of fundamental importance<sup>15</sup>; we have accordingly advised objective manufacturers to facilitate development for CLARITY samples, and these new objectives are becoming available.

In addition to optimized detection optics, the nature of the microscopy system is important for achieving high imaging speed and minimizing photobleaching. Although confocal and two-photon microscopes have been the workhorse systems in volumetric imaging for the reasons described above, over the past two decades light-sheet fluorescence microscopy has emerged as a powerful approach for high-speed volumetric imaging. **Figure 3b** compares the mechanistic foundations of these three imaging modalities. Confocal and two-photon microscopy are point-scanning techniques, which detect optical signals point-by-point to construct an image. Confocal microscopy achieves optical sectioning by the use of a pinhole at the detection focal plane to reject out-of-focus light, whereas two-photon microscopy uses the fact that only simultaneous absorption of two photons results in fluorescence emission, an event that is much more likely to occur at the point of highest light intensity in the sample (the focal plane). Light-sheet microscopy, in contrast, builds on a hundred-year-old idea to illuminate the sample from the side with a thin sheet of light, and to detect the emitted fluorescence signal with an in-focus orthogonally arranged



**Figure 5** | Ultrafast imaging of whole mouse brain using COLM. (a) Volume rendering of a whole mouse brain data set acquired from an intact clarified Thy1-eYFP mouse brain using COLM. **b–d** illustrate internal details of the intact mouse brain volume visualized by successive removal of occluding dorsal-side images. The brain was perfused with 0.5% (wt/vol) acrylamide monomer solution, and clarified passively at 37 °C with gentle shaking. Camera exposure time of 20 ms was used, and the RI liquid 1.454 was used as immersion medium. The entire data set was acquired in ~4 h using a 10×, 0.6-NA objective. **Supplementary Video 1** demonstrates visualization of the data set at high resolution.



objective<sup>16,17</sup>. The optical sectioning is achieved by the confinement of illumination to a selective plane, which allows the use of fast charge-coupled device (CCD) or scientific complementary metal-oxide semiconductor (sCMOS) cameras to capture the whole image simultaneously, and results in an increase of 2–3 orders of magnitude in imaging speed compared with confocal and two-photon microscopy. Moreover, light-sheet microscopy minimizes photobleaching (**Fig. 3b**) by confining illumination to the plane of interest. Taken together, these properties of light-sheet microscopy may be well suited for the imaging of large clarified samples, consistent with previously demonstrated utility for minimizing unnecessary illumination in living cells<sup>15</sup>, embryos<sup>18–20</sup> and large conventional histology samples<sup>8,21</sup>.

### Overview of procedure

We describe here protocols for CLARITY. Before starting the CLARITY process, reagents are prepared (Step 1) and animals are anesthetized (Step 2). The entire CLARITY process is termed clarification, and it includes HM infusion and cross-linking (Steps 3–8), thermally triggered hydrogel polymerization (Steps 9–11), passive or active lipid clearing (Steps 12–14) and RI homogenization (Step 20). If required, samples are immunostained (Steps 15–19) before the RI homogenization. The clarified samples are then deep-imaged using optimized objectives, adapted confocal methodologies and COLM (**Fig. 4**). The entire depth of the mouse brain (>5 mm) can be imaged at high resolution using CLARITY-optimized optics (**Figs. 5–8**; **Supplementary Videos 1–3**); we show here application of the new generation of CLARITY-optimized objectives now available from the major commercial sources, including Leica and Olympus, which are specifically adapted to lipid-extracted clarified tissue.

The extensive lipid removal intrinsic to CLARITY appears to be essential not only for transparency but also for achieving efficient antibody penetration throughout intact brains; this stringent de-lipidation would normally be a destructive process causing extensive loss of biological molecules<sup>13</sup>, but it is enabled by the hydrophilic hydrogel-tissue hybrid in a way that also

preserves fine processes and ultrastructure even over multiple rounds of staining and elution<sup>13</sup>. Many variations are possible and will continue to be explored; the ‘CUBIC’ screen<sup>14</sup> recently provided an intriguing diversity of additional hydrophilic lipid solubilization reagents including amino alcohols that can be used in CLARITY protocols<sup>14</sup>, although it was noted that the amino alcohols incubation leaves behind substantial lipid content in the tissue<sup>14</sup>, such that lipid-rich structures including white matter remain partially opaque and the approach may not allow antibody penetration for molecular labeling and resolution of fine processes deeper than 0.5–0.8 mm into mature brain tissue<sup>14</sup>. The electrophoretic tissue clearing (ETC) process (although not essential even for whole-mouse-brain CLARITY, as shown here in the 3-week passive-CLARITY approach, which achieves full transparency and antibody access) still accelerates de-lipidation and might therefore help enhance an amino alcohols approach to CLARITY, although this remains to be seen and will depend on the size and charge of the resulting lipid-containing particles.

Both the speed of delipidation and the speed of imaging are crucial for CLARITY, which is driving the development of COLM. For high-speed collection of imaging data from large clarified volumes, COLM is 100–1,000 times faster than conventional scanning methods, leading to vastly decreased photobleaching (**Figs. 5 and 6**; **Supplementary Videos 1 and 2**). The properties of COLM not only are useful for mouse brains but also will be particularly relevant for maintaining this high cellular and subcellular resolution at practical speeds in brains from larger-brained organisms.

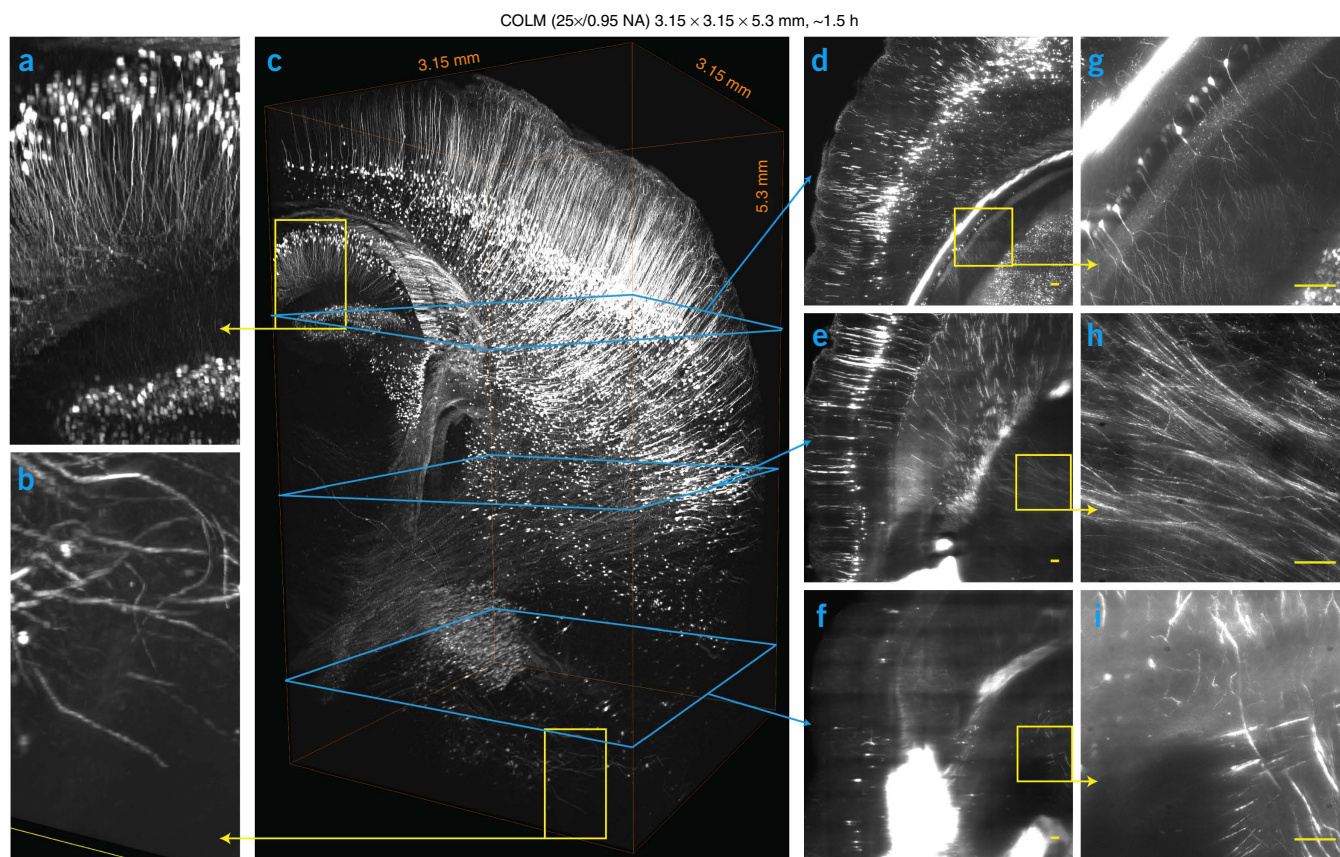


**Figure 6** | Fast high-resolution imaging of clarified brain using COLM. 3.15 mm × 3.15 mm × 5.3 mm volume acquired from an intact clarified Thy1-eYFP mouse brain using COLM with 25× magnification; the brain had been perfused with 0.5% (wt/vol) acrylamide monomer solution. The complete image data set was acquired in ~1.5 h; for optimal contrast, the lookup table (LUT) of zoomed-in images was linearly adjusted between panels. (a,b) Magnified views from panel c region defined by yellow boxes. (d–i) Maximum-intensity projections over a 50-μm-thick volume, as shown by the progression of cyan and yellow boxes and arrows. Camera exposure time of 20 ms was used; RI liquid 1.454 was used as the immersion medium. High-resolution details of the data set are provided in **Supplementary Video 2**. Scale bars, 100 μm.

The fast COLM approach described here for clarified intact mouse brains maintains high resolution even 5–6 mm deep in tissue using the 0.95-NA objective; ultimate resolution in any light microscope

remains limited by the laws of diffraction ( $\lambda/2NA = \sim 180$  nm), but the emergence of super-resolution (or ‘diffraction unlimited’) imaging methods, such as STED/RESOLFT and PALM/STORM (see recent review<sup>22</sup>), could in the future allow a further 4–5-fold improvement in achievable resolution.

As a final comment for future work, we note that very large data sets result from this new capability for high-speed imaging of large tissue volumes at high resolution, and extensive innovation will be needed in image analysis and data management (for example, if the intact 0.3-cc mouse brain is represented by  $0.5 \times 0.5 \times 0.5$  cubic-micrometer 16-bit voxels, at least 4.8 terabytes of raw data result). Fortunately, big-data and high-performance computing have led to advanced image-compression technologies such as JPEG 2000 3D, increased computational

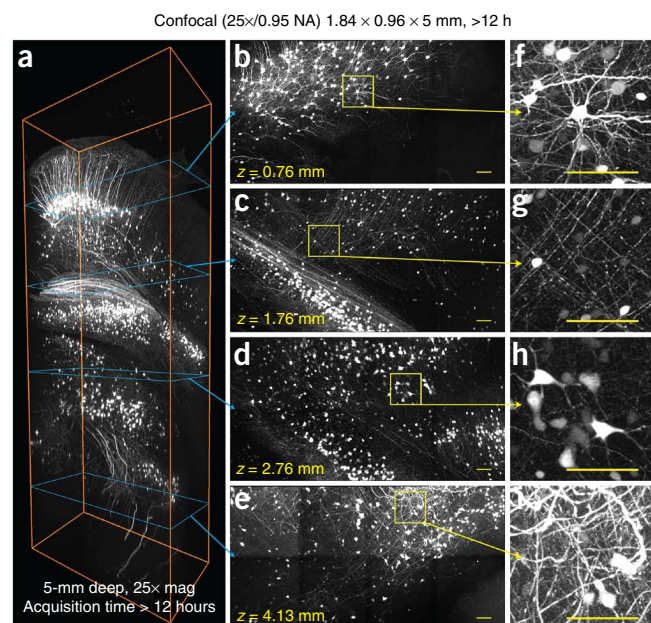
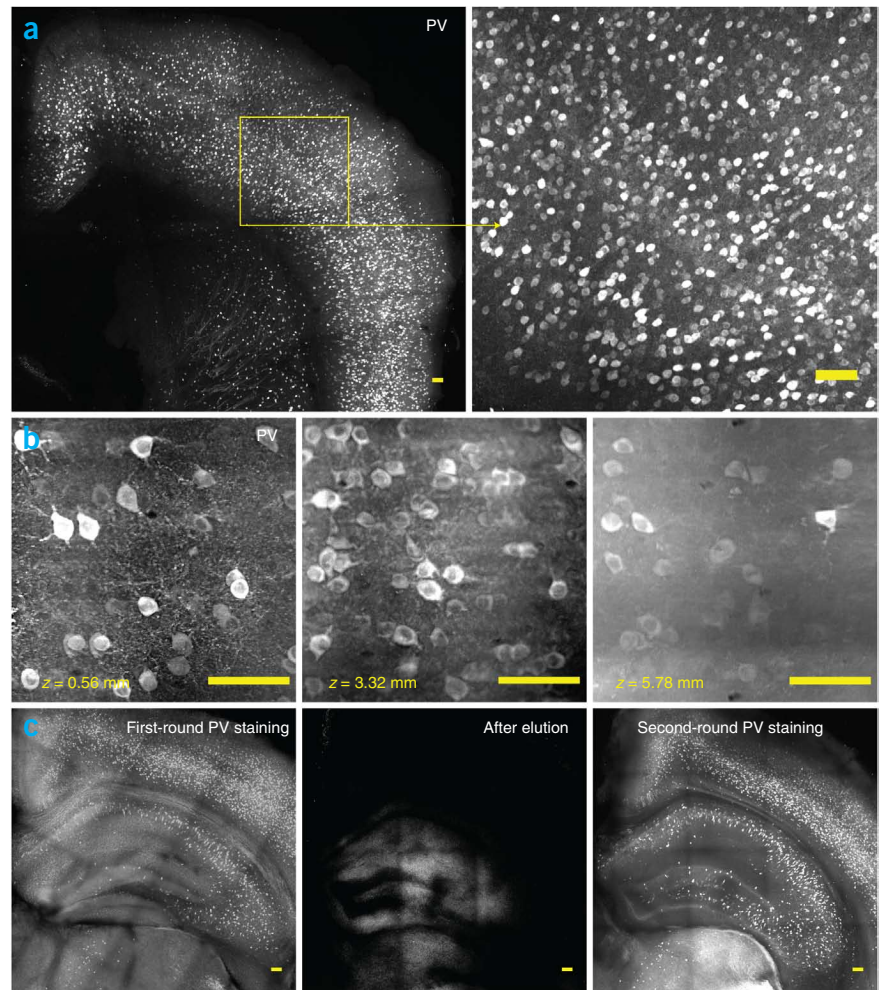


**Figure 7** | Optimized confocal microscopy of clarified samples. 1.837 mm × 0.959 mm × 5 mm volume imaged from an intact cleared Thy1-eYFP mouse brain using a confocal microscope at 25× magnification. Brain was perfused with 4% (wt/vol) acrylamide monomer solution. (a) Rendering of entire volume. Images were acquired in top-to-bottom direction, corresponding to the dorsoventral brain axis. (b–e) Maximum-intensity z-projections (1 mm, 1 mm, 1 mm, 1.7 mm in thickness, respectively) at different imaging depths as marked by cyan arrows. (f–i) Magnified images of the regions marked by yellow boxes in b–e. **Supplementary Video 3** details a 3D rendering of the entire volume. Scale bars, 100 μm.



**Figure 8 |** Molecular interrogation of clarified tissue. **(a)** Parvalbumin (PV)-positive neurons in a 1-mm-thick tissue block of mouse brain, labeled using anti-PV antibody. The brain was perfused with 4% (wt/vol) acrylamide monomer solution. The tissue block was imaged using confocal microscopy. Images represent maximum intensity projections. **(b)** Whole-brain immunostaining to label all PV-positive neurons in an intact mouse brain. Panels show labeled cells at different depths in the sample. The brain was perfused with 4% (wt/vol) acrylamide monomer solution and clarified passively. The intact brain was imaged using COLM with a 25× objective. **(c)** Multiple rounds of immunostaining in the same tissue block (1% (wt/vol) acrylamide monomer solution). Left to right, first round of immunostaining for PV, followed by label elution via overnight (~12 h) incubation in clearing buffer at 60 °C; this was, in turn, followed by a second round of immunostaining for PV. DAPI present in the first round was successfully eluted as well (not shown). All images represent maximum z-projections. Scale bars, 100 μm.



capacity with GPU parallel computation technology and cloud infrastructures (such as Amazon S3) for data storage and sharing. We expect that the integration and application of these methods to CLARITY will allow increasingly complete access to, and understanding of, the molecular and structural organization of large intact tissues.

## MATERIALS

### REAGENTS

- Sample to be imaged. This protocol describes imaging of brain samples prepared from adult Thyl-eYFP or wild-type (WT) mice
- **CAUTION** Experiments on animals must conform to all relevant governmental and institutional regulations.
- Beuthanasia-D Special (Merck Animal Health)
- **HM solution**
- Acrylamide solution (40% (wt/vol); Bio-Rad, cat. no. 161-0140)
- **CAUTION** Acrylamide monomers are toxic. Perform all procedures in a fume hood.
- Bisacrylamide solution (2% (wt/vol); Bio-Rad, cat. no. 161-0142)
- **CAUTION** Bisacrylamide is toxic. Perform all procedures in a fume hood.
- Paraformaldehyde (16% (wt/vol); Electron Microscopy Sciences, cat. no. 15710-S) **CAUTION** PFA is toxic. Perform all procedures in a fume hood.
- Polymerization thermal initiator VA044 (Wako, cat. no. VA-044)
- 10× PBS

### Clearing solution

- Boric acid (Sigma-Aldrich, cat. no. B7901)
- Sodium hydroxide pellets (EMD, cat. no. SX0590-3)
- SDS (Sigma-Aldrich, cat. no. L337 or Amresco, cat. no. 0837)

### Refractive index matching and imaging solution

- FocusClear (CeExplorer Labs)
- MountClear (CeExplorer Labs)
- Glycerol (87%, vol/vol)
- Custom RI liquids (RI 1.454, Cargille Labs, cat. no. 1806Y)

### Immunostaining reagents

- PBS, 1× with Triton X-100 (0.1%, vol/vol)
- Primary and secondary antibodies (see **Table 1** for examples of antibodies we have used)

### EQUIPMENT

#### Hydrogel polymerization

- Vacuum pump (Buchi, cat. no. V-700)
- Desiccation chamber (any)
- Nitrogen supply (any)

#### ETC chambers

- 60-ml Nalgene bottles for one-brain ETC chamber (Thermo Scientific, cat. no. 2118-0002)
- 125-ml Nalgene bottle for four-brain ETC chamber (Thermo Scientific, cat. no. 2118-0004)
- Push-to-connect fittings for constructing ETC chamber (McMaster-Carr, cat. no. 9087K14)
- Platinum wire, 0.5 mm (Sigma-Aldrich, cat. no. 267201-2G)
- Banana plug (Invitrogen, cat. no. EI9021)
- Sample holder (BD Falcon, cat. no. 352340)
- Mesh to fix sample orientation (McMaster-Carr, cat. no. 9275T38)
- Power supply (Bio-Rad, cat. no. 164E5052)
- Power supply adapter (Bio-Rad, cat. no. 164E5064)
- Water circulator (Lauda Brinkmann, cat. no. RE 415)
- Tubings (McMaster-Carr)
- Filters (McMaster-Carr, cat. no. 4448K35)
- Adhesive (McMaster-Carr, cat. no. 746A17)

**TABLE 1** | Antibodies for staining a 1-mm-thick tissue block in 1 ml of PBST.

Volume ( $\mu$ l)	Antibody	Supplier
10–20	Anti-TH	Abcam, no. ab113 or affinity-purified anti-TH (Abcam, no. ab51191) for lower background)
10–20	Anti-PV	Abcam, no. ab32895 or Abcam, no. ab11427
5–10	Anti–glial fibrillary acidic protein (GFAP)	Abcam, no. ab53554
5–20	Anti–synapsin-1	Abcam, no. ab64581
10–20	Anti–postsynaptic density protein 95 (PSD-95)	Abcam, no. ab2723 or Abcam, no. ab12093
10–20	Anti–myelin basic protein (MBP)	Aves, no. MBP
5–10	Anti–somatostatin	Peninsula, no. T-4103
5–10	Anti–choline acetyltransferase (ChAT)	Millipore, no. ab144p
10–20	Anti-GFP	Invitrogen, no. A21311, Alexa conjugated; Invitrogen, no. A3185, Alexa conjugated; Invitrogen, no. G10362
20	Anti–microtubule-associated protein 2 (MAP-2)	Abcam, no. ab32454
10	Anti-neurofilament	Aves, nos. NFL, NFM or NFH

#### Sample mounting and imaging if using a confocal microscope

- Wellco dish (Pelco (Ted Pella), cat. no. 14032E120)
- BluTack Putty
- Kwik-Sil (World Precision Instruments, cat. no. KWIKESIL)
- Microscope slides
- Coverslips
- Confocal microscope. The results shown here were obtained using an Olympus FV1200 microscope
- CLARITY-optimized objectives (now available from major commercial sources such as Leica or Olympus) **Figure 7** and **Supplementary Video 3** show results obtained using a 25 $\times$ , 0.95-NA, 8-mm WD objective resulting in a 5-mm-deep stack. **Figure 8a,c** shows results obtained using a water-immersion 10 $\times$ , 0.6-NA, 3-mm WD objective

#### REAGENT SETUP

**HM solution** Prepare 400 ml of HM solution by mixing 40 ml of 40% (wt/vol) acrylamide (4% (wt/vol) final concentration), 10 ml of 2% (wt/vol) bisacrylamide (0.05% (wt/vol) final concentration), 40 ml of 10 $\times$  PBS, 100 ml of 16% (wt/vol) PFA (4% (wt/vol) final concentration), 210 ml of distilled water and 1 g of VA-044 thermal initiator (0.25% (wt/vol) final concentration). Keep all the reagents on ice; divide 40 ml of the HM solution into aliquots in 50-ml conical tubes and store them at  $-20^{\circ}\text{C}$  until needed (several weeks). Acrylamide and bisacrylamide concentration in HM solution can be proportionally reduced to speed up the clearing process. We have successfully used concentrations of 0.5%/0.0125% acrylamide/bisacrylamide ranging up to 4.0%/0.05%; however, we recommend lower acrylamide/bisacrylamide concentrations to start with, as the clearing speed is increased several-fold. Lower concentrations should increase the pore size of the hydrogel and hence also allow faster diffusion of antibodies, but at the potential cost of increased biomolecular content loss in the clearing process. Higher concentrations could provide better preservation for biomolecules, but they may lead to slower tissue clearing and immunohistochemistry time.

**SDS/borate clearing (SBC) buffer** Prepare stocks of 20% (wt/vol) SDS (in  $\text{H}_2\text{O}$ ) and 1 M boric acid buffer (pH adjusted to 8.5). These stocks can be stored at room temperature ( $25^{\circ}\text{C}$ ) for several weeks. Final clearing buffer is freshly prepared by diluting 20% (wt/vol) SDS and 1 M boric acid buffer fivefold in distilled water.

#### EQUIPMENT SETUP

**ETC setup (optional).** A detailed schematic and photographs are shown in **Figure 2**. Construct ETC chambers (i) by inserting two zig-zag-shaped

platinum wire electrodes, bound to banana plugs, at the bottom of the Nalgene bottles, and (ii) by inserting two push-to-connect fittings to provide the inlet for SBC buffer (in the Nalgene bottle body) and the outlet (in the center of the bottle lid). A soldering rod can be used to create appropriate holes by melting the plastic, and strong epoxy adhesives can be used to glue electrodes and inlet/outlet push-to-connect fittings. Two different sizes of Nalgene bottles can be used for making one- or four-sample clearing chambers.

Use appropriate tubing (e.g., 1/2- and 3/8-inch outer diameter tubes) to connect the ETC chambers to a refrigerated circulator. A water filter should also be used to keep the buffer free of any particles. Tube fitting manifolds can be used to collect multiple ETC chambers to a single buffer circulator. By using four of the four-sample ETC chambers, up to 16 mouse brains can be cleared in less than 1 week with one circulator.

Regular monitoring of critical parameters such as buffer temperature, flow rate, pH and electric current flow levels should be performed either manually or by using automated real-time readouts. **Figure 2** summarizes the entire ETC setup. **CLARITY-optimized light-sheet microscopy** A light-sheet microscope consists of a standard wide-field detection optical arm, which includes the detection objective, the tube lens and a camera, and the orthogonally arranged independent illumination arm consisting of a low-NA objective, a tube lens and either a cylindrical lens to generate a static light sheet or a galvanometer scanner/f-theta lens for creating dynamic light sheets with Gaussian or Bessel beams<sup>8,18,23–25</sup>. Conventional light-sheet microscopy suffers from image quality degradation owing to out-of-focus scattered light; several methods have been developed to help reject out-of-focus light in the light sheet (at some cost in imaging speed, increased photobleaching and instrumentation complexity), such as structured illumination<sup>25,26</sup>.

We developed COLM to maximize the compatibility of clarified samples with light-sheet microscopy, using CLARITY objectives (25 $\times$  and 10 $\times$ , Olympus), a fast sCMOS camera, two-axis galvo scanners along with the f-theta lens, a low-NA objective to generate dynamic light sheets using a Gaussian beam, an optimized sample chamber (detailed in the following section) and an xyz-theta sample mount stage that provides a long travel range of 45 mm in each of the dimensions to allow imaging of large samples (**Fig. 4**). The control electronics design and parts for COLM are summarized in **Supplementary Figure 2**. COLM uses synchronized illumination detection to improve imaging quality, especially at higher depths (**Fig. 4c**), thereby exploiting the unidirectional readout (as opposed to standard bi-directional



## PROTOCOL

readout, albeit at the cost of imaging speed) mode available in the next-generation sCMOS cameras. The scanning beam (which creates the dynamic light sheet) is synchronized with the unidirectional single-line readout of the emitted signal, resulting in a virtual confocal-slit arrangement, which rejects out-of-focal-plane signal owing to scattering deeper in the sample. Automated-alignment parameter calibration (using linear adaptation) in COLM corrects for misalignment artifacts across the whole sample space (Fig. 4d); the corresponding control software is available on request.

**Sample mounting apparatus for COLM** The final component of COLM is a CLARITY-optimized sample mounting strategy that minimizes optical inhomogeneity along the detection path (Fig. 4b). Clarified whole mouse brain (or any large clarified intact tissue, such as a spinal cord) is mounted in a cuvette made of fused quartz glass (standard cuvettes used for spectrophotometry measurements) filled with FocusClear; note that the RI of fused quartz (~1.458) is nearly identical to that of FocusClear. By using a bottom adapter (Fig. 4b), the sample cuvette is mounted onto the xyz-theta stage

inside the sample chamber (Fig. 4b). The much larger chamber is then filled with a relatively economically priced custom RI matching liquid (RI 1.454, Cargille Labs, cat. no. 1806Y), resulting in an optically homogeneous sample manipulation system. RI liquid costs several hundred dollars per half liter, which is enough to fill the sample chamber (and more than an order of magnitude cheaper than FocusClear); it can be reused many times. The chamber also can be filled with 87% (vol/vol) glycerol, which is workable but is highly viscous and more likely to cause and maintain inhomogeneities such as gradients and bubbles in large volumes.

**Computational workstation for data analysis** As the image data sizes are expected to be very large, it is important to use a computational workstation with abundant RAM, multicore CPUs and an excellent graphics card. Data shown here were handled on a workstation with the following configuration: Intel server board S2600CO, two Intel Xeon E5-2687W 8C CPUs, ~130 GB of DIMM RAM, an ~8-TB hard disk (Seagate Savvio 10K), a NVidia K5000 graphics card and a high-resolution monitor (NEC MultiSync PA301W, 30 inch, 2,560 × 1,600).

## PROCEDURE

### Transcardial perfusion of mouse brain with HM solution

1| Prepare the HM stock solution by thawing frozen vials on ice or in a refrigerator. Gently mix the thawed monomer solution by inverting. Keep all reagents on ice during the whole procedure. Note that Steps 2–4 take ~30 min.

▲ **CRITICAL STEP** Make sure that there is no precipitation floating in the monomer solution; this is an indicator of spontaneous polymerization of the stored monomer solution.

### ? TROUBLESHOOTING

2| Anesthetize the mice by injecting Beuthanasia-D (100 mg/kg of body mass).

! **CAUTION** Follow appropriate institutional guidelines for handling animals.

3| Perfuse the mice with 20 ml of ice-cold 1× PBS at ~10 ml/min. Make sure that the PBS becomes colorless by the end of perfusion. If not, repeat the washing step with an additional 20 ml of PBS.

4| Perfuse the animal with HM solution at ~10 ml/min. Recover the brain (or other tissues) from the animal and place it in the remaining 20 ml of HM solution. Incubate the sample at 4 °C for a minimum of 1 d. Protect the sample from light if fluorophores are present.

! **CAUTION** PFA and acrylamide monomer are toxic. Perform all procedures in a fume hood.

▲ **CRITICAL STEP** Stiffening of muscles is indicative of successful perfusion.

■ **PAUSE POINT** Tissues can be kept at 4 °C for up to 2 d.

### Preparation for tissue embedding

▲ **CRITICAL** Residual oxygen must be removed from the tissue sample. This section (Steps 5–8) describes how to degas the conical tube that contains the tissue sample using a standard vacuum pump and desiccation chamber, as well as a nitrogen gas supply.

5| Place the 50-ml conical tube on a rack in the desiccation chamber. Partially open the cap to allow gas exchange.

! **CAUTION** PFA and acrylamide monomer are toxic. Perform Steps 5–8 in a fume hood.

6| Open the nitrogen tank main valve and adjust the control valve to fill the desiccation chamber with nitrogen gas. Next, toggle the desiccation chamber valve from the nitrogen gas in-flow to the vacuum pump outlet.

7| Turn on the vacuum pump. Verify that the chamber is under full vacuum by testing the chamber lid. Keep it running for 10 min.

8| Switch the vacuum pump off; the nitrogen will slowly fill the chamber. Carefully open the chamber just enough to reach the tubes, and then tighten the lids while continuously purging with nitrogen gas.

▲ **CRITICAL STEP** Oxygen inhibits hydrogel polymerization. Therefore, make sure to remove as much residual oxygen as possible.

## Tissue embedding by hydrogel polymerization

**9|** Transfer the air-tight closed conical tube to a 37 °C room or to a water bath for 3–4 h. Gentle shaking helps in heat transfer for achieving robust and uniform polymerization.

**▲ CRITICAL STEP** Make sure that the hydrogel has fully solidified before proceeding to the next step. If not, repeat the degassing section (Steps 5–8) and transfer the tube to 37 °C again. Note that lower acrylamide concentration (such as 0.5% (wt/vol)) hydrogels do not solidify fully upon polymerization. Therefore, the degassing step is especially crucial.

**10|** Carefully extract the brain (or other tissues) from solidified hydrogel by softly rubbing all the hydrogel from the surface. Kimwipes can be used to remove the residual gel from the tissue surface.

**! CAUTION** Hydrogel waste disposal should be conducted according to local regulations for HMs and cross-linkers (e.g., acrylamide and PFA).

**11|** Wash the tissue sample twice with 50 ml of SBC buffer for 24 h at room temperature to dialyze the remaining PFA, initiator and monomer. If desired, the tissue sample can be cut into ~1–2-mm blocks immediately after embedding for accelerated clearing and staining, as described below.

### ? TROUBLESHOOTING

**■ PAUSE POINT** The brain sample can be left in SBC buffer for up to 4 weeks at 37 °C until clearing.

## Tissue clearing by passive thermal diffusion or by ETC

**▲ CRITICAL** For successful completion of lipid removal, it is important to tune the clearing parameters to tissue properties and dimensions. With ETC, tissue orientation relative to the electric field is important; to minimize the distance traveled by SDS micelles and to maximize SDS flux, tissue blocks or organs should be oriented with the shortest axis parallel to the electric field direction. Whenever allowed by speed, tissue properties and other constraints, we advise passive thermal clearing rather than ETC.

**12|** Start clearing tissue passively (option A) or using ETC (option B) (ETC is faster, but it can damage tissue and reduce immunostaining efficacy).

### ? TROUBLESHOOTING

#### (A) Passive clearing of hydrogel-embedded tissue (passive CLARITY)

- (i) Gently shake the sample at 37 °C. Higher temperatures up to 60 °C can be used for faster clearing, but this may quench endogenous fluorescence in cases where that is a relevant consideration. The passive clearing process can also be sped up while retaining its key advantages by using lower concentrations of acrylamide/bisacrylamide in the HM solution, as discussed in Reagent Setup.

#### (B) ETC of hydrogel-embedded tissue

- (i) Transfer the sample to an ETC chamber, as shown in **Figure 2**. Use mesh sheets to fix the orientation of tissue relative to the electric field direction, and then close the chamber as shown in **Figure 2**. Up to four brain samples can be cleared in one ETC chamber, and up to 16 in one multiplexed setup (**Fig. 2**).
- (ii) Turn ON the clearing solution refrigerated circulator first, and then switch ON the power supply. Different combinations of voltage and buffer temperature can be used for the ETC process. For adult mouse brain samples, we recommend running the ETC process at 25 V and 37 °C for ~3–5 d, with regular checks on pH of the clearing buffer; immediately change the buffer if the pH drops below 7.5.
 

**▲ CRITICAL STEP** Power input into the ETC chamber results in heat generation in the solution, which needs to be dissipated by the circulating clearing solution. In general, higher temperature and voltage result in faster clearing of the tissue, but they may lead to a higher risk of sample, epitope or fluorescence loss (see also ref. 27 for detailed characterization of the effect of temperature on SDS micelle sizes).

**13|** Check for completion of tissue clearing by assessing for transparency (easy visualization of high-contrast signals such as a black-and-white grid or printed text through the tissue) and homogeneity (even distribution of transparency across the tissue; **Supplementary Fig. 1**). Once the tissue is clearer, proceed to the next step.

**14|** Wash the tissue twice in PBST or boric acid buffer (0.2 M/pH 8.5 with 0.1% (vol/vol) Triton X-100) for 1 d at 37 °C. For whole-brain CLARITY, we recommend not only low-percentage (1%, wt/vol) acrylamide monomer and thorough passive clearing in SDS but also a wash in boric acid buffer/0.1% (vol/vol) Triton X-100 (instead of PBST) to remove the remaining SDS.

### ? TROUBLESHOOTING

## Molecular labeling

**▲ CRITICAL** A tissue sample may have endogenous transgenic expression of fluorophores to label molecular and structural details in the sample, but immunohistochemistry can also be used to label structures and molecules of interest. Follow this

## PROTOCOL

section for immunostaining a thick tissue block or intact mouse brain. If you do not wish to perform immunohistochemistry, proceed directly to Step 21.

**15|** Ensure that the tissue has been washed thoroughly in PBST (or boric acid buffer/0.1% (vol/vol) Triton X-100 wash for whole brains) for at least 1 d at 37 °C (as described in Step 14). As immunostaining should typically be conducted in PBST, transfer the brain from boric acid/0.1% (vol/vol) Triton X-100 to PBST 30 min before incubation with primary antibody (Step 16, below).

### ? TROUBLESHOOTING

**16|** Incubate in primary antibody/PBST solution (beginning with 1:50 dilution) for 2 d at 37 °C for tissue blocks, or for up to a week for the whole intact brain. Note that ~0.2 M borate/0.1% (vol/vol) Triton X-100 buffer (pH 8.5), in some cases, can also be used in place of PBST for antibody incubations to reduce background staining. As with any staining procedure, it is important to systematically optimize staining conditions (detergent, temperature, concentrations and so on) for the particular antibody used. **Table 1** lists examples of antibodies that we have used to incubate a 1-mm-thick block in 1 ml of solution<sup>13</sup>: A whole mouse brain can be incubated in 5 ml of solution with scaled-up antibody volumes supplemented periodically; for example, 50 µl of anti-tyrosine hydroxylase (anti-TH) antibody as above can be added, followed by 20 µl more every 2 d for ~1 week.

**! CAUTION** Make sure that there is no microbial growth during long incubations at 37 °C; 0.01% (wt/vol) sodium azide can be added to the primary and secondary antibody solutions.

**▲ CRITICAL STEP** High antibody concentrations (1:20–1:100) are usually required for effective immunostaining to ensure deep penetration into tissue and to overcome the large aggregate number of antibody binding sites over the volume. 1:1,000 dilutions typically lead to inadequate tissue penetration. A second major factor for successful immunostaining is complete removal of lipids during clearing.

**17|** Wash off the primary antibodies with PBST buffer at 37 °C for 1 d for tissue blocks and for 2–3 d for whole brain (refresh buffer every 4–6 h).

**18|** Incubate with the desired secondary antibody (1:50–1:100) in PBST for 2 d at 37 °C for tissue blocks or for up to 1 week for whole brain. Note that a nuclear labeling dye, such as DAPI (1 µg/ml), can also be added at this step.

**19|** Wash off the secondary antibodies with PBST at 37 °C for 1 d for tissue blocks and 2–3 d for whole brain.

**■ PAUSE POINT** The sample can be stored in PBST (with 0.01% (wt/vol) sodium azide) at 4 °C for up to a week.

**20|** To prepare for imaging, transfer the tissue into FocusClear for RI homogenization, as described below. Note that it is possible to elute (remove) prior labels by incubating in clearing buffer at 60 °C overnight (**Fig. 8c**) in preparation for another round of labeling after imaging has been performed. Once labels have been removed, repeat Steps 15–19 with alternative antibodies.

### Refractive index homogenization

**▲ CRITICAL** Owing to inherent RI inhomogeneity of tissues, photons (both the excitation light and the emitted fluorescence signal) scatter when traveling through the sample, limiting the quality of images that can be acquired, as well as the imaging depth that can be achieved. Therefore, a crucial final part of sample preparation is the homogenization of the microscopic environment inside the tissue using a chemical solution that matches closely the average RI of the tissue. FocusClear (CelExplorer Labs) and 85–87% (vol/vol) glycerol have been extensively tested<sup>13</sup> for this purpose; both promote tissue transparency but currently the best results are achieved with FocusClear<sup>13</sup>.

**21|** Transfer the PBST-washed tissue into FocusClear (or 87% (vol/vol) glycerol), and periodically check the visual clarity of the sample over the next few hours. 1- or 2-mm-thick tissue blocks will typically complete the RI homogenization process in ~1 h, whereas an intact mouse brain can take several hours. Treatment at 37 °C accelerates this process several-fold but may damage the sample; room temperature treatment is gentler. Once the tissue has been fully clarified, immediately proceed with imaging preparations (described below) or return the tissue to PBST.

**■ PAUSE POINT** Before RI homogenization (or after), the tissue may be stored indefinitely in PBST (with 0.01% (wt/vol) sodium azide) at 4 °C, but extended incubation of tissue in FocusClear is not advised, as this can result in the formation of a white opaque precipitation that will hinder deep imaging.

### Imaging and analysis

**22|** CLARITY allows access to deep tissues using multiple light microscopy modalities; we describe here protocols for deep imaging of clarified tissues using advanced confocal (option A) and light-sheet microscopies (option B) (**Figs. 3–8**). As confocal microscopes are widely available, we include an optimized procedure to image through the entire depth of a clarified intact mouse brain with confocal methods. Most of these principles will apply similarly to the other imaging modalities; indeed, we also discuss the high-speed, high-resolution light-sheet microscopy of clarified samples, and present data sets to demonstrate compatibility.

### ? TROUBLESHOOTING



## (A) Confocal imaging

- (i) *Sample mounting.* Mount a whole clarified mouse brain between two Wellco dishes as follows. First place a Wellco dish upside down, with the glass surface facing up. Prepare a 7–10-mm-thick-diameter uniform cylindrical tube of BluTack putty clay by smoothly rubbing between gloved hands. Use the putty tube to create a well on the glass surface by folding it in a circle, leaving a small opening on joining ends. Place the clarified brain carefully inside this well, preferably with the dorsal surface up.
- (ii) Place another Wellco dish on top of the well such that the glass side directly interfaces with the putty walls. Gently press on the top Wellco dish until the glass touches the brain surface, while keeping the two glass surfaces parallel. Make sure that the putty sticks well to the glass surfaces to avoid any leaks afterward.
- (iii) Use the small joint opening in the putty wall to fill it up with FocusClear using a 1,000- $\mu$ l pipette. Seal this hole by using Kwik-Sil silicone adhesive, and leave it to dry for ~30 min, after which the sample is ready for imaging.  
**▲ CRITICAL STEP** An important advantage of this sample mounting procedure is that it allows imaging from either side. Thick brain blocks can be mounted similarly using thinner putty walls, and even thinner slices (<2 mm) can be mounted using a standard glass slide and coverslip with a thin well of putty.
- (iv) Select an appropriate objective. The NA of the detection objective determines the maximum resolution that can be achieved. **Figure 3a** shows plots of diffraction-limited lateral and axial resolutions as a function of NA. For a NA of 0.9, the optics can at best achieve ~0.278- $\mu$ m lateral resolution and ~1.235- $\mu$ m axial resolution (along the z axis). The Nyquist sampling criterion suggests that the detected pixel size of the microscope should at least be twofold smaller than the resolution of the optics. Thus, for a 25 $\times$  objective, optimal imaging will be achieved by adjusting pixel sampling (controlled by changing the number of pixels collected) such that the pixel size is  $0.278/2 = 0.139 \mu\text{m}$ , and the z-spacing is  $1.235/2 = \sim 0.617 \mu\text{m}$ . These settings will take full advantage of the objective capability, but the high pixel sampling density will slow imaging speed considerably. This tradeoff between image quality and imaging speed should be assessed for each system on the basis of the constraints of the biological question.
- (v) Determine the desired laser intensity. This is another crucial parameter. High laser power will photobleach the sample quickly; therefore, especially for large tissue volumes, power should be minimized. Although this may reduce the signal level, the signal can also be improved without increasing laser intensity by increasing the electronic gain, although higher gain may result in higher noise. Increasing pixel dwell time will also increase the signal, but at the cost of increased imaging time and photobleaching.
- (vi) Select and add an appropriate immersion liquid between the glass dish and the microscope objective. The immersion liquid should ideally match the specifications of the microscope objective. For example, when a water-immersion objective is used, only water should be present between the glass and the objectives. However, if the RI of the immersion liquid is much different from that of the mounting liquid (such as FocusClear), optical aberrations may result, which become substantial for deep imaging with high-NA objectives. As a rule, the more closely the RIs match, the better the image quality. Therefore, we show here the use of a custom CLARITY-corrected objective for high-resolution deep imaging at 25 $\times$  (**Fig. 7**) in an optimized custom immersion oil with a RI of 1.454 (Cargille Labs, cat. no. 1806Y), matching the RI of FocusClear. We also describe the use of a water-immersion 10 $\times$  objective for high image quality in a clarified and immunostained tissue block (**Fig. 8a,c**).
- (vii) Commence confocal imaging. As the field of view of a microscope objective is often smaller than the sample itself, it may be necessary to collect multiple stacks in tiling arrangements, which are then stitched together to yield a large image volume. Many microscope objectives suffer from vignetting (in which the image quality is lower at the edges than in the middle). This artifact in the stitched images can be avoided by using a digital zoom of ~1.2 during imaging.

## (B) COLM

- (i) Mount the sample (e.g., intact mouse brain) in a quartz cuvette of appropriate dimensions, so that the sample remains stationary while imaging (**Fig. 4b**). Note that many different sizes of quartz cuvettes are available from vendors (such as Starna Cells); however, if the sample does not fit easily a small piece of acrylamide gel (or similar transparent material) can be used to provide structural padding on the side opposite to the imaging side. For adult mouse brain, we recommend either 10  $\times$  5 mm or 10  $\times$  10 mm base cuvettes with padding, depending on the age of the mouse; these are standard sizes, but custom sizes can also be purchased from many vendors.
- (ii) Fill the cuvette with FocusClear, just enough to cover the entire sample. Use an adapter to mount the cuvette on the xyz-theta stage (**Fig. 4b**).  
**▲ CRITICAL STEP** Avoid bubbles or dust particles, as they will interfere with the imaging.
- (iii) Set the tiling parameters. Some samples can be larger than the field of view of the objective used, and therefore they will require tiling of image stacks to cover the entire sample. To specify the number of tiles, begin by defining the coordinates of the two opposite corners of the region of interest; we recommend 15–20% tile overlap. As with confocal imaging, specify the start and end z-position of the stack by finding the first and last image frames containing useful signal from the sample, and then set the desired z-step value.

PROTOCOL

- (iv) Adjust for any misalignment of the light sheet and the detection focal plane, which (particularly during imaging of large samples) can result in blurred images. To do this, optimize the light-sheet and focal-plane alignment parameters over the entire sample space, as defined in Step 22B(iii). We achieve this by optimizing these parameters at every millimeter of the tissue for all the tiles, and then by linearly interpolating the values for z-steps in between these millimeter steps. Optimal parameters are identified by finding maxima in a specified neighborhood corresponding to the image quality measure; to automate this process, we implement an optical focus-quality measure, as the ratio of high frequency and low frequency signal in Fourier space.
- (v) Initiate the imaging experiment and data collection.

3D reconstruction and analysis

**23 |** Perform 3D reconstructions either with commercial software (e.g., Imaris from Bitplane or Amira) or via free or open-source projects (e.g., Vaa3D, [www.vaa3d.org](http://www.vaa3d.org)). Typically, commercial software tools can be easier to use, although they can be quite costly compared with open-source versions. The stitching of tiles of image stacks can either be performed using the microscope control software or open-source modules (e.g., the stitching plug-in in Fiji<sup>28</sup>, XuvTools<sup>29</sup>, Vaa3D plug-in<sup>28,30</sup> or TeraStitcher<sup>31</sup>). For the sample results shown here, the stitching of tiles was performed with TeraStitcher (for COLM) or the Fiji stitcher plug-in (for confocal microscopy). Similarly, manual or semiautomatic tracing of neuronal morphology can be performed using specific modules in commercial software such as Imaris and Amira, or with open-source tools such as Neuromantic<sup>32</sup>.

? TROUBLESHOOTING

Troubleshooting advice can be found in **Table 2**.

**TABLE 2 |** Troubleshooting table.

Step	Problem	Possible reason	Possible solution
Hydrogel embedding (Steps 1–11)	Transcardiac perfusion is not possible (for example, in human tissue samples)		Passively infuse the monomers into postfixed tissue by incubating the sample in hydrogel monomer solution at 4 °C for several days (depending on the tissue size) with gentle shaking. For example, 3–4 d of passive infusion is sufficient for a pre-fixed mouse brain
	The hydrogel polymerizes	Hydrogel can polymerize at room temperature	Keep the tubing and needles on ice during perfusion to prevent clogging. It is also crucial to use ice-cold PBS to chill the tissues before perfusing them with the hydrogel monomer solution
ETC clearing (Steps 12–14)	Poor tissue clearing	The two electrodes may be placed too far away from each other	Keep them as close as possible, without touching the sample. This is necessary to create the highest current density to drive tissue clearing
		Overpolymerization of the hydrogel	Do not leave the sample in the monomer solution (at 37 °C) for more than 5–6 h. If the samples are polymerized overnight, this will make tissue clearing and staining very difficult
		Clearing buffer needs to be refreshed	The SBC buffer needs to be refreshed once the pH goes below 7.5 or clearing efficiency will drop. The use of increased voltage or larger electrodes will increase the rate of buffer consumption; therefore, the buffer may need to be changed more frequently under these conditions
	Tissue damage during clearing: black deposits on samples and electrodes	Black deposits will form on the cathode over time (on the order of several days), and will gradually start to transfer to the tissue surface, if left unattended	The electrodes can be easily cleaned by reversing the voltage polarity, and running the power and buffer flow for 10–20 minutes. Regular cleaning of electrodes (every 3–4 d) will prevent black deposits on the samples

(continued)

**TABLE 2** | Troubleshooting table (continued).

Step	Problem	Possible reason	Possible solution
ETC clearing (Steps 12–14)	Tissue damage during clearing: Sample burned or turned yellow	High temperature (resulting from higher current and/or insufficient heat dissipation due to low flow rate) will cause yellowness or may even burn or melt the samples	Individual users must determine the optimal combination of voltage, temperature and flow rate settings on the basis of the sample properties and chamber design
	Loss of fluorescence	High temperature or voltage can quench fluorescence, as can high acidity	It is crucial to maintain the temperature at 37 °C and the pH above 7.5
	White precipitate formation after FocusClear treatment	An opaque white deposit may form inside samples left in FocusClear for more than 1–2 d	Any residual SDS from the clearing solution substantially accelerates this deposition. It is very important to completely remove residual SDS by thoroughly washing the samples with PBST (0.1–0.2% (vol/vol) Triton X-100) several times over 1–2 d (refresh PBST at least every day). In general, samples should never be stored in FocusClear, but returned to PBST at 4 °C as soon as imaging is completed
Staining and imaging (Steps 15–22)	Low staining reagent or label penetration	Tissue sample is not very well cleared in terms of lipid removal	Clearing can be further improved by passively clearing the samples in SBC solution (at 37 °C with gentle shaking) for additional days after ETC. Note that whenever feasible, perform passive thermal clearing for tissue destined for subsequent immunostaining
		Poor antibody penetration	Up to 1% (vol/vol) Triton X-100 (more typically 0.2–0.5%) in PBS can be employed to facilitate further antibody penetration
		Insufficient incubating solution	Use large volumes of incubating solutions for big tissue samples. Frequent refreshment of the buffer and antibody can lead to further improvement
	Heavy background or weak signal	Samples that become damaged during ETC tend to have high autofluorescence background	Refer to the previous section for preventing sample damage. Note also that ETC is not always necessary for small tissue samples, and prolonged passive clearing can be a very suitable option in many cases
		Long incubation in FocusClear can lead to fine precipitation (invisible to the naked eye) that generates heavy autofluorescence	FocusClear treatment should be kept to the minimum needed, and residual SDS must be removed from the samples
		Photobleaching	To prevent photobleaching, minimize any unnecessary light exposure to the sample before and during imaging. Keep laser power to a minimum while setting up the imaging parameters for the tissue

### ● TIMING

Steps 1–4, infusion of HM solution: 1 d

Steps 5–11, hydrogel polymerization and tissue washing: 1 d

Steps 12–14, tissue clearing: 5 d (ETC) to 3 weeks (passive thermal clearing) for 1% (wt/vol) acrylamide HM solution-embedded whole adult mouse brain



Steps 15–20, immunostaining, single round: 1–2-mm tissue block: 2–3 d with a labeled primary antibody or 5–6 d for conventional two-step primary/secondary antibody stain; whole mouse brain: 7–10 d with a labeled primary antibody or 2–3 weeks for conventional two-step primary/secondary antibody stain

Step 21, RI homogenization: 4–5 h

Step 22, imaging: 3 h–3 d

Step 23, stitching and 3D reconstruction: 1 h–1 d

## ANTICIPATED RESULTS

**Figure 4c** compares the images taken using standard light-sheet microscopy or COLM. We performed imaging of whole-brain samples from mice using 10× or 25× magnification objectives (**Figs. 5** and **6**; **Supplementary Videos 1** and **2**). Multiple factors contribute to image quality at this whole-brain level; for example, independent of imaging modality, the sample needs to be clarified extremely well with minimum tissue damage, and the detection optics including objective must be well corrected for expected optical aberrations, even with confocal or two-photon methods.

CLARITY allows molecular and structural interrogation of tissue by allowing deep imaging of transgenic and/or biochemically labeled tissue samples. As discussed above, to achieve the best imaging quality, careful preparation of the sample and the optical setup is crucial. First, as demonstrated in **Figure 3**, key relevant properties of the objective must be considered, including NA, WD, color correction and RI correction. Several commercial objectives are available that possess high NA (>1.0) and color correction at multiple wavelengths, but at the cost of WD; conversely, longer-WD objectives are available at the cost of the NA. We explored the emerging commercially available and custom solutions and found that it is indeed possible to achieve deep high-resolution and overall high-quality imaging in clarified samples (**Figs. 5–8**; **Supplementary Videos 1–3**). For example, **Figure 7** presents a 5-mm-deep brain volume, spanning the dorsal to the ventral surface of the mouse brain, acquired using a confocal microscope and a CLARITY-optimized 25×, 0.95-NA objective (Olympus). Other water-immersion, oil-immersion or air objectives may also prove to be useful for quality imaging deep in tissue.

The major limitations of confocal and two-photon microscopes are (i) slow speed owing to point-scanning mechanisms (**Fig. 3**) and (ii) damage to tissues and fluorophores due to redundant illumination of the whole sample for every optical plane imaged, thus limiting the size of the sample that can be imaged in a reasonable time frame before the sample is completely photobleached (particularly in the case of confocal microscopy). Although it is not as severe as with confocal, it is well documented (and particularly relevant here for long imaging times) that two-photon microscopy also leads to photobleaching and other nonlinear tissue damage<sup>33–35</sup>. Light-sheet microscopy now emerges as an alternative for fast 3D imaging of large clarified samples, as described below.

We assessed the compatibility of clarified samples with light-sheet microscopy, observing an imaging speed greater than two orders of magnitude faster than confocal microscopy with minimal photobleaching; for example, it was possible to image an entire mouse brain in ~4 h using a 10× magnification objective and in ~1.5 d using a 25× objective, as opposed to many days and months, respectively, with a confocal microscope. COLM is especially well suited for the interrogation of large tissue samples labeled with transgenic or histochemical approaches. The increased speed of acquisition and higher quality of data generated via CLARITY using new microscopy methods, combined with high-speed CLARITY processing itself and enabled by the parallelized and efficient tissue transformation protocols described here, together define a versatile and efficient platform for structural and molecular interrogation of large and fully assembled tissues.

*Note: Any Supplementary Information and Source Data files are available in the online version of the paper.*

**ACKNOWLEDGMENTS** We thank the entire Deisseroth laboratory for helpful discussions and Anna Lei for technical assistance. K.D. is supported by the Defense Advance Research Projects Agency (DARPA) Neuro-FAST program, the National Institute of Mental Health (NIMH), the National Science Foundation (NSF), the National Institute on Drug Abuse (NIDA), the Simons Foundation and the Wiegers Family Fund. All CLARITY tools and methods described are distributed and supported freely (<http://clarityresourcecenter.org>, <http://wiki.claritytechniques.org>) and discussed in an open forum (<http://forum.claritytechniques.org>).

**AUTHOR CONTRIBUTIONS** R.T. and K.D. wrote the paper with input from L.Y. on the content. R.T., L.Y. and B.H. prepared the clarified samples, and R.T. developed the imaging framework. K.D. supervised the project.

**COMPETING FINANCIAL INTERESTS** The authors declare no competing financial interests.

Reprints and permissions information is available online at <http://www.nature.com/reprints/index.html>.

1. Bock, D.D. *et al.* Network anatomy and *in vivo* physiology of visual cortical neurons. *Nature* **471**, 177–182 (2011).
2. Briggman, K.L., Helmstaedter, M. & Denk, W. Wiring specificity in the direction-selectivity circuit of the retina. *Nature* **471**, 183–188 (2011).
3. Conchello, J.A. & Lichtman, J.W. Optical sectioning microscopy. *Nat. Methods* **2**, 920–931 (2005).
4. Helmchen, F. & Denk, W. Deep tissue two-photon microscopy. *Nat. Methods* **2**, 932–940 (2005).
5. Tang, J., Germain, R.N. & Cui, M. Superpenetration optical microscopy by iterative multiphoton adaptive compensation technique. *Proc. Natl. Acad. Sci. USA* **109**, 8434–8439 (2012).
6. Micheva, K.D., Busse, B., Weiler, N.C., O'Rourke, N. & Smith, S.J. Single-synapse analysis of a diverse synapse population: proteomic imaging methods and markers. *Neuron* **68**, 639–653 (2010).
7. Ragan, T. *et al.* Serial two-photon tomography for automated *ex vivo* mouse brain imaging. *Nat. Methods* **9**, 255–258 (2012).
8. Dodt, H.U. *et al.* Ultramicroscopy: three-dimensional visualization of neuronal networks in the whole mouse brain. *Nat. Methods* **4**, 331–336 (2007).
9. Hama, H. *et al.* Scale: a chemical approach for fluorescence imaging and reconstruction of transparent mouse brain. *Nat. Neuroscience* **14**, 1481–1488 (2011).

10. Ke, M.T., Fujimoto, S. & Imai, T. SeeDB: a simple and morphology-preserving optical clearing agent for neuronal circuit reconstruction. *Nat. Neuroscience* **16**, 1154–1161 (2013).
11. Kim, S.Y., Chung, K. & Deisseroth, K. Light microscopy mapping of connections in the intact brain. *Trends Cognit. Sci.* **17**, 596–599 (2013).
12. Erturk, A. *et al.* Three-dimensional imaging of solvent-cleared organs using 3DISCO. *Nat. Protocols* **7**, 1983–1995 (2012).
13. Chung, K. *et al.* Structural and molecular interrogation of intact biological systems. *Nature* **497**, 332–337 (2013).
14. Susaki, E.A. *et al.* Whole-brain imaging with single-cell resolution using chemical cocktails and computational analysis. *Cell* **157**, 726–739 (2014).
15. Planchon, T.A. *et al.* Rapid three-dimensional isotropic imaging of living cells using Bessel beam plane illumination. *Nat. Methods* **8**, 417–423 (2011).
16. Siedentopf, H. & Zsigmondy, R. Über Sichtbarmachung und Größenbestimmung ultramikroskopischer Teilchen, mit besonderer Anwendung auf Goldrubingläser. *Ann. Phys.* **10**, 1–39 (1903).
17. Huisken, J. & Stainier, D.Y. Selective plane illumination microscopy techniques in developmental biology. *Development* **136**, 1963–1975 (2009).
18. Huisken, J., Swoger, J., Del Bene, F., Wittbrodt, J. & Stelzer, E.H. Optical sectioning deep inside live embryos by selective plane illumination microscopy. *Science* **305**, 1007–1009 (2004).
19. Tomer, R., Khairy, K., Amat, F. & Keller, P.J. Quantitative high-speed imaging of entire developing embryos with simultaneous multiview light-sheet microscopy. *Nat. Methods* **9**, 755–763 (2012).
20. Krzic, U., Gunther, S., Saunders, T.E., Streichan, S.J. & Hufnagel, L. Multiview light-sheet microscope for rapid *in toto* imaging. *Nat. Methods* **9**, 730–733 (2012).
21. Santi, P.A. *et al.* Thin-sheet laser imaging microscopy for optical sectioning of thick tissues. *BioTechniques* **46**, 287–294 (2009).
22. Hell, S.W. Microscopy and its focal switch. *Nat. Methods* **6**, 24–32 (2009).
23. Greger, K., Swoger, J. & Stelzer, E.H. Basic building units and properties of a fluorescence single plane illumination microscope. *Rev. Sci. Instrum.* **78**, 023705 (2007).
24. Keller, P.J., Schmidt, A.D., Wittbrodt, J. & Stelzer, E.H. Reconstruction of zebrafish early embryonic development by scanned light-sheet microscopy. *Science* **322**, 1065–1069 (2008).
25. Keller, P.J. *et al.* Fast, high-contrast imaging of animal development with scanned light sheet-based structured-illumination microscopy. *Nat. Methods* **7**, 637–642 (2010).
26. Kalchmair, S., Jahrling, N., Becker, K. & Dodt, H.U. Image contrast enhancement in confocal ultramicroscopy. *Optics Lett.* **35**, 79–81 (2010).
27. Hammouda, B. Temperature effect on the nanostructure of SDS micelles in water. *J. Res. Natl. Inst. Stand. Technol.* **118**, 151–167 (2013).
28. Peng, H., Ruan, Z., Long, F., Simpson, J.H. & Myers, E.W. V3D enables real-time 3D visualization and quantitative analysis of large-scale biological image data sets. *Nat. Biotechnol.* **28**, 348–353 (2010).
29. Emmenlauer, M. *et al.* XuvTools: free, fast and reliable stitching of large 3D datasets. *J. Microscopy* **233**, 42–60 (2009).
30. Yu, Y. & Peng, H. Automated high speed stitching of large 3D microscopic images. *Biomedical Imaging: From Nano To Macro, 2011 IEEE International Symposium On March 30–April 2, 2011, Chicago* 238–241 (2011).
31. Bria, A. & Iannello, G. TeraStitcher: a tool for fast automatic 3D-stitching of teravoxel-sized microscopy images. *BMC Bioinformatics* **13**, 316 (2012).
32. Myatt, D.R., Hadlington, T., Ascoli, G.A. & Nasuto, S.J. Neuromantic: from semi-manual to semi-automatic reconstruction of neuron morphology. *Front. Neuroinform.* **6**, 4 (2012).
33. Patterson, G.H. & Piston, D.W. Photobleaching in two-photon excitation microscopy. *Biophys. J.* **78**, 2159–2162 (2000).
34. Hopt, A. & Neher, E. Highly nonlinear photodamage in two-photon fluorescence microscopy. *Biophys. J.* **80**, 2029–2036 (2001).
35. Koester, H.J., Baur, D., Uhl, R. & Hell, S.W. Ca<sup>2+</sup> fluorescence imaging with pico- and femtosecond two-photon excitation: signal and photodamage. *Biophys. J.* **77**, 2226–2236 (1999).